

Optimizing Privacy-Preserving Outsourced Convolutional Neural Network Predictions

Minghui Li, Sherman S. M. Chow, Shengshan Hu, Yuejing Yan, Minxin Du, and Zhibo Wang

Abstract—Neural networks provide better prediction performance than previous techniques. Prediction-as-a-service thus becomes popular, especially in the outsourced setting since it involves extensive computation. Recent researches focus on the privacy of the query and results, but they do not provide model privacy against the model-hosting server and may leak partial information about the results. Some of them further require frequent interactions with the querier or heavy computation overheads. This paper proposes a new scheme for privacy-preserving neural network prediction in the outsourced setting, *i.e.*, the server cannot learn the query, (intermediate) results, and the model. Similar to SecureML (S&P'17), a representative work which provides model privacy, we leverage two non-colluding servers with secret sharing and triplet generation to minimize the usage of heavyweight cryptography. Further, we adopt asynchronous computation to improve the throughput, and design garbled circuits for the non-polynomial activation function to keep the same accuracy as the underlying network (instead of approximating it). Our experiments on four neural network architectures show that our scheme achieves an average of 282 \times improvements in reducing latency compared to SecureML. Compared to MiniONN (CCS'17) and EzPC (EuroS&P'19), both without model privacy, our scheme achieves a lower latency by a factor of 18 \times and 10 \times , respectively. For the communication costs, our scheme outperforms SecureML by 122 \times , MiniONN by 49 \times , and EzPC by 38 \times times.

Index Terms—Convolutional neural network, outsourcing computation, privacy preservation, homomorphic encryption

1 INTRODUCTION

NEURAL network (NN) [1] identifies and models relationships underlying a set of data. Convolutional neural networks (CNN), based on biologically-inspired variants of multi-layer perceptrons, are proven to be very useful in medical image analysis, natural language processing, and recognition of images and videos. The trained network is a valuable asset generated after collecting and learning from a massive amount of data. It is tempting for an adversary to steal the model, pirate it, or use it to provide a commercial prediction service for profits [2]. Moreover, with the knowledge of the model, the risk of compromising the model privacy is higher since white-box attacks can infer more information than black-box attacks, *e.g.*, membership inference attack [3], [4], [5] for determining if a specific sample was in the training dataset. Knowing the model also makes adversarial example attacks [6], [7], [8], [9] more effective. A tiny perturbation of the input can deceive the model and threaten its accuracy. Outsourcing the model and the prediction service to any third-party cloud server (say, for relieving from the cost of maintaining an online server) thus comes with great privacy and security implications. This paper aims to ensure *model privacy*, *i.e.*, protecting the model privacy not only from the querier (as most of the existing works did) but also from the hosting server.

- *M. Li, S. Hu, Y. Yan, and Z. Wang are with the School of Cyber Science and Engineering, School of Computer Science, Wuhan University, Wuhan, 430072, China, and State Key Laboratory of Cryptology, P.O. Box 5159, Beijing, 100878, China.*
E-mail: {minghui, hushengshan, yjyan, zbwang}@whu.edu.cn
- *S. Chow and M. Du are with the Department of Information Engineering, The Chinese University of Hong Kong, Hong Kong. E-mail: {sherman, dm018}@ie.cuhk.edu.hk*

1.1 Related Work

Privacy-Preserving Prediction without Model Privacy. Many existing schemes protect the privacy of the *query* from the server. Yet, they consider the model owner is the server performing the prediction tasks, *i.e.*, the prediction service only works with the *plaintext knowledge of the model*. Some works [10], [11] use additive homomorphic encryption to perform operations over the encrypted query and the clear model. Others [12], [13], [14], [15], [16] design secure two-party computation (S2C) protocols for various kinds of machine-learning computations. The S2C approach often expects the queriers to remain online and interact with the server continuously, thus bringing some burden to the queriers and incurring higher network round-trip time.

Fully Homomorphic Encryption (FHE). FHE [17] allows processing (any polynomial functions over) encrypted data. It is thus a handy tool for not only processing the query in an encrypted format but also processing over an encrypted model. As a counterexample, in the case of decision tree, Tai *et al.* [18] managed to use only additive HE instead of FHE to support S2C evaluation, but it is subject to the limitation that the server needs to know the model in clear. As a versatile tool, FHE operations are not cheap. It also fails to cover common non-polynomial operations in NN. CryptoDL [19] and E2DM [20] approximate them by polynomials, which degrades the prediction accuracy. Also, this approach requires the model owner to encrypt the model w.r.t the public key of each querier. Not only it does not scale when there are multiple queriers, but also allows any querier to decrypt the model. For the specific case of outsourced decision-tree evaluation a very recent work [21] uses multi-key FHE, *i.e.*, the decryption requires multiple secret keys and thus involves multiple parties.

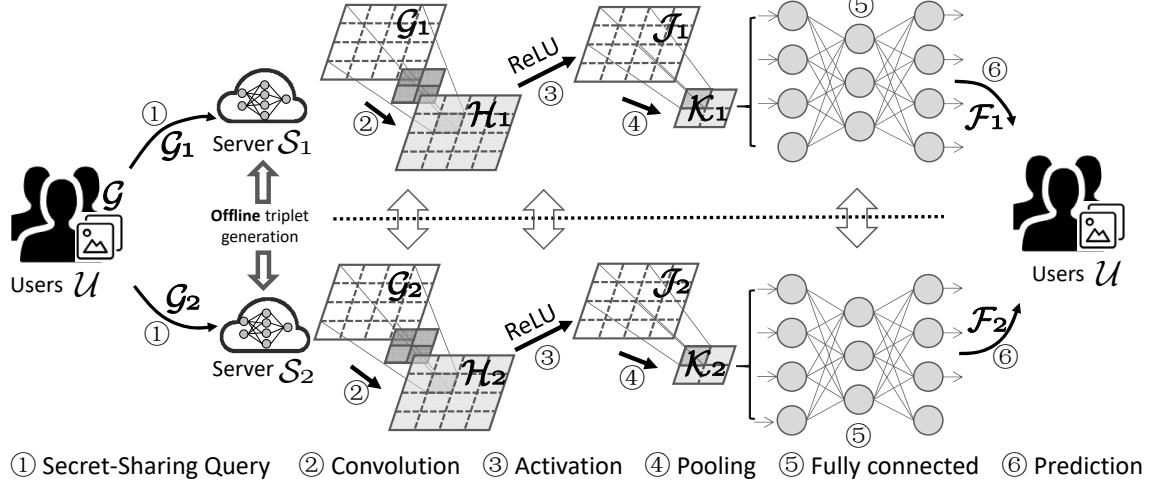


Fig. 1: System overview

Secret Sharing and Non-Colluding Computation Model. To reduce the use of (relatively heavyweight) cryptographic techniques, many works [22], [23], [24] exploited the non-colluding assumption. In the minimal setting with two non-colluding (cloud) servers, neither of them is trusted; yet, they are assumed not to be colluding with each other.

Baryalai *et al.* [25] realize prediction services by S2C among two servers, one with the model and the other one with a secret key. They do not consider the privacy of the intermediate data (*e.g.*, the output of the activation function), which may allow inference of prediction results.

SecureML [26] additively shares the model into two shares and deploys them respectively to two servers. The querier also shares the query across the two servers. The two servers interact with each other, and derive their corresponding share of the prediction result eventually. The user can then obtain the final result by merging both shares locally. To speed up the online (inner-product) computation, SecureML generates Beaver’s multiplication triplet [27] for additive sharing in an offline preprocessing stage. For the non-polynomial operation (*i.e.*, comparison), they use Yao’s garbled circuits (GC) [28] for boolean computations. Yet, SecureML only focuses on simple neural networks (and linear/logistic regression).

Table 1 coarsely compares existing schemes. It is fair to say that there is no outsourcing solution with model privacy and satisfactory performance in accuracy and efficiency.

1.2 Technical Highlights

This paper studies privacy-preserving neural network prediction. Our contributions are summarized below.

- We design protocols for different phases of the convolutional neural network prediction. Our system can simultaneously protect the query, the model, any intermediate results, and the final prediction results against the servers while guaranteeing a high accuracy and efficiency.
- We accelerate the triplets generation [26], [27] using data packing and single-instruction-multiple-data (SIMD) [29]. Besides, we adopt asynchronous

computation to speed up both offline and online computations.

- For non-polynomial activation functions, we design a series of garbled circuits for S2C between the two servers. This preserves the accuracy differing from existing approaches which only approximate the activation functions by polynomial.
- For efficiency, we replace the non-polynomial max-pooling function with the linear average-pooling function. Our experimental result of training via these two methods demonstrates that the final accuracy of average-pooling is comparable or even higher than that of max-pooling.
- Our extensive experiments on four neural network architectures show that our scheme achieves 282 \times , 18 \times , and 10 \times lower latency than SecureML [26], MiniONN [12], and EzPC [15], respectively. For the communication costs, our scheme outperforms prior art such as SecureML by 122 \times , MiniONN by 49 \times , and EzPC by 38 \times .
- We provide a security analysis in the simulation paradigm to show the privacy of our scheme.

2 PROBLEM STATEMENT AND PRELIMINARY

2.1 System Model and Threat Model

Fig. 1 illustrates our system model. The model, generated by a model owner (not depicted), is randomly split and shared between two servers, S_1 and S_2 . A user U who holds the query also randomly splits it into two shares and uploads them to S_1 and S_2 , respectively. Based on the shared model and query, S_1 interacts with S_2 to make predictions. After interactions, the servers obtain the corresponding shared results and return them to U , who can eventually recover the real prediction result locally.

Following [25], [26], [12], [13], [14], [15], [16], we assume that S_1 and S_2 are honest-but-curious and do not collude with each other. Most service providers (*say*, Microsoft Azure and Amazon EC2) are motivated to maintain their reputation instead of risking it with collusion. With this

TABLE 1: Comparison of related work

	Privacy			Accuracy	Efficiency
	model para.	inter. data	query		
NDCS [25]	✗	✗	✓	High	Low
CryptoNets [10]	✗	✓	✓	Low	Medium
CryptoDL [19]	✓	✓	✓	Low	Medium
E2DM [20]	✓	✓	✓	Low	Medium
XONN [16]	✗	✓	✓	Medium	High
Deepsecure [14]	✗	✓	✓	High	Medium
SecureML [26]	✓	✓	✓	High	Medium
MiniONN [12]	✗	✓	✓	High	High
Gazelle [13]	✗	✓	✓	High	High
EzPC [15]	✗	✓	✓	High	High
Our Scheme	✓	✓	✓	High	High

assumption, our design goal becomes ensuring both \mathcal{S}_1 and \mathcal{S}_2 cannot learn any information about the prediction model, the query from \mathcal{U} , and the (intermediate) prediction results. Intuitively, this gives us hope for higher efficiency without greatly affecting accuracy.

2.2 Convolutional Neural Network (CNN) and Notations

We use image processing as the running example since CNN is good for such task [30]. A typical CNN consists of four classes of layers. The core one is the *convolutional layer*. It computes the convolution, essentially an *inner product*, between the raw pixel values in each local region of the image and a set of the convolutional kernel. Let \mathcal{G} be the query image as an $n \times n$ matrix of 8-bit pixel. For simplicity, we consider only one convolution kernel \mathcal{C} each of size $m \times m$ (*i.e.*, the padding mode is “same”). The convolution transforms \mathcal{G} into a matrix \mathcal{H} .

It is usually the *activation layer* after the convolutional layer. It applies an element-wise *non-polynomial* activation function for increasing the nonlinear properties of the model. We use the most fashionable ReLU function, which only keeps the positive part of any real-valued input (*i.e.*, $f(x) = \max(0, x)$). We let \mathcal{J} be the image activated by $f(x)$, which remains of size $n \times n$.

The *pooling layer* performs a down-sampling along the spatial dimensions while retaining the critical information. The usual ones are *max-pooling* and *average-pooling*, which outputs the maximum or the average value of the pool, respectively. The size of the pool is $q \times q$. The resulting smaller image \mathcal{K} is of size $(n/q)^2$.

The final layer is the *fully-connected layer*. The image matrix in the previous layer is first transformed into a column vector of dimension being the neuron numbers of the first layer in fully-connected layer, *i.e.*, each element in the vector is the input of the corresponding neuron. Every neuron in the previous layer is connected to every neuron in the next layer. The weight matrix of the fully-connected layer is denoted by \mathcal{W} . By the scalar product of the output

TABLE 2: Notations

\mathcal{G}	the original image (of pixel size $n \times n$)
\mathcal{C}	the $(m \times m)$ convolutional kernels of CNN
\mathcal{H}	the convoluted image
$f(x)$	the non-polynomial activation function
\mathcal{J}	the activated image
$q \times q$	the size of the pooling window
\mathcal{K}	the down-sampled image
\mathcal{W}	the weight matrix in fully-connected layer
\mathcal{F}	the prediction results
\cdot	the inner product operation

of the previous layer and the corresponding weight matrix, we obtain a column vector, each of its element corresponds to the input of the next layer. The output of the last layer is deemed as the final prediction results.

The classes with the desired scores form the final prediction results \mathcal{F} , which correspond to the most probable categories. The goal of our system is to let the querier learn \mathcal{F} without revealing the query \mathcal{G} to the servers or the neural network to the servers.

We tabulate the notation in Table 2. We operate on the secret-shared values extensively. For differentiation, we use a superscript 1 or 2 to denote the shared information of servers \mathcal{S}_1 or \mathcal{S}_2 . For examples, the shared image held by \mathcal{S}_1 and \mathcal{S}_2 are \mathcal{G}^1 and \mathcal{G}^2 respectively, and the i -th row and j -th column entry held by \mathcal{S}_1 are $\mathcal{G}_{i,j}^1$. The inner product operator is \cdot . For the inner product of two matrices, we first transform the matrices into vectors.

2.3 Cryptographic Tools

2.3.1 Homomorphic Encryption (HE)

HE (*e.g.*, [17], [31]) allows computations over encrypted data without access to the secret key. Decrypting the resultant ciphertexts gives the computation result of the operations as if they had been performed on the plaintext. For the public/private-key pair (pk, sk) , and an encryption of x denoted by $\llbracket x \rrbracket_{pk}$, we have homomorphisms \oplus and \otimes where $\llbracket a \rrbracket_{pk} \oplus \llbracket b \rrbracket_{pk} = \llbracket a + b \rrbracket_{pk}$, $\llbracket a \rrbracket_{pk} \otimes \llbracket b \rrbracket_{pk} = \llbracket a \times b \rrbracket_{pk}$. Following MiniONN [12], this work uses the ring-based FHE scheme called YASHE [31]. It offers a plaintext space which is large enough for usual computation. With single-instruction multiple-data (SIMD) techniques [29], 4096 independent plaintexts in our application can be packed to one ciphertext and operated in parallel, which reduces the communication and computation.

2.3.2 Secure Two-Party Computation (S2C)

S2C allows two parties to jointly compute a function over their private inputs while warranting the correctness. No party learns anything about the other’s input beyond what is implied by the function. *Garbled circuits* proposed by Yao [28] can evaluate arbitrary function represented as a boolean circuit. At a high level, one party prepares the garbled circuit and sends it to the other party, who

$\text{tri} \leftarrow \text{TRIP}(a_1, b_1, (pk, sk); a_2, b_2, pk)$

Input: \mathcal{S}_1 holds the shares $a_1 \in \mathbb{Z}_{2^t}$, $b_1 \in \mathbb{Z}_{2^t}$ and the key pair (pk, sk) . \mathcal{S}_2 holds the other shared $a_2 = (a - a_1) \bmod 2^t$, $b_2 = (b - b_1) \bmod 2^t$ and the public key pk .

Output: \mathcal{S}_1 gets $\text{tri}^1 = (a_1, b_1, z_1)$. \mathcal{S}_2 gets $\text{tri}^2 = (a_2, b_2, z_2)$, where $z = z_1 + z_2 = a \cdot b \bmod 2^t$.

At \mathcal{S}_1 side:

- 1) Encrypt a_1 and b_1 to have $\llbracket a_1 \rrbracket_{pk}$ and $\llbracket b_1 \rrbracket_{pk}$;
- 2) Send the ciphertexts $\llbracket a_1 \rrbracket_{pk}$ and $\llbracket b_1 \rrbracket_{pk}$ to \mathcal{S}_2 .

At \mathcal{S}_2 side:

- 1) Compute $V_1 = \llbracket a_1 \cdot b_2 \rrbracket_{pk} = \llbracket a_1 \rrbracket_{pk} \otimes \llbracket b_2 \rrbracket_{pk}$,
 $V_2 = \llbracket a_2 \cdot b_1 \rrbracket_{pk} = \llbracket b_1 \rrbracket_{pk} \otimes \llbracket b_1 \rrbracket_{pk}$;
- 2) Send $V_3 = V_1 \oplus V_2 \oplus \llbracket r \rrbracket_{pk}$ to \mathcal{S}_1 , where $r \in \mathbb{Z}_{2^t}$;
- 3) Set $z_2 = (a_2 \cdot b_2 + r) \bmod 2^t$.

At \mathcal{S}_1 side:

- 1) Decrypt V_3 to have $v = a_1 \cdot b_2 + a_2 \cdot b_1 + r$;
- 2) Set $z_1 = (v + a_1 \cdot b_1) = (a \cdot b + r) \bmod 2^t$.

The triplet is $\text{tri} = ((a_1, a_2), (b_1, b_2), (z_1, z_2))$.

Fig. 2: Secure triplet generation protocol

$(\mathcal{H}^1; \mathcal{H}^2) \leftarrow \text{CONV}(\mathcal{G}^1, \mathcal{C}^1, (pk, sk); \mathcal{G}^2, \mathcal{C}^2, pk)$

Input: \mathcal{S}_1 holds the shares of image \mathcal{G}^1 and convolutional kernel \mathcal{C}^1 , and (pk, sk) , \mathcal{S}_2 holds shares $\mathcal{G}^2, \mathcal{C}^2$, and pk .

Output: $\mathcal{S}_1, \mathcal{S}_2$ get shared convoluted images $\mathcal{H}^1, \mathcal{H}^2$ resp.

\mathcal{S}_1 and \mathcal{S}_2 :

- 1) **for** i, j **in** range n
 - Choose the sub-image $\langle \mathcal{G}_{p,q}^1 \rangle_{p,q=i-\frac{m-1}{1}}^{p,q=i+\frac{m-1}{1}}$ as vector $\tilde{\mathcal{G}}_{i,j}^1$ and $\langle \mathcal{G}_{p,q}^2 \rangle_{p,q=i-\frac{m-1}{1}}^{p,q=i+\frac{m-1}{1}}$ as vector $\tilde{\mathcal{G}}_{i,j}^2$;
 - Call TRIP to generate the triplet vectors: $\text{tri} = (A_1 = \langle a_1^k \rangle, A_2 = \langle a_2^k \rangle, B_1 = \langle b_1^k \rangle, B_2 = \langle b_2^k \rangle, Z_1 = \langle z_1^k \rangle, Z_2 = \langle z_2^k \rangle)_{k=1}^m$;
 $// z_1^k + z_2^k = (a_1^k + a_2^k)(b_1^k + b_2^k)$ or $Z_1 + Z_2 = AB$
 - \mathcal{S}_1 sends $U^1 = \tilde{\mathcal{G}}_{i,j}^1 - A_1, V^1 = \mathcal{C}^1 - B_1$ to \mathcal{S}_2 ,
 \mathcal{S}_2 sends $U^2 = \tilde{\mathcal{G}}_{i,j}^2 - A_2, V^2 = \mathcal{C}^2 - B_2$ to \mathcal{S}_1 ;
 - \mathcal{S}_1 and \mathcal{S}_2 compute $U = \tilde{\mathcal{G}}_{i,j} - A, V = \mathcal{C} - B$;
 - \mathcal{S}_1 computes $\mathcal{H}_{i,j}^1 = -UV + \tilde{\mathcal{G}}_{i,j}^1 V + \mathcal{C}^1 U + Z_1$,
 \mathcal{S}_2 computes $\mathcal{H}_{i,j}^2 = \tilde{\mathcal{G}}_{i,j}^2 V + \mathcal{C}^2 U + Z_2$.
- 2) Return \mathcal{H}^1 and \mathcal{H}^2 .
 $\mathcal{H}^1 + \mathcal{H}^2 = Z_1 + Z_2 + \mathcal{G}C - AB$.

Fig. 3: Convolution operation

obliviously obtains the circuit and then evaluate the entire circuit gate-by-gate. During the entire process, no party learns anything about the input data of others beyond what is implied by the final results.

Secret Sharing allows one to distribute a secret among several parties by distributing shares to each party. For example, in (t, n) -Shamir secret sharing [32], there are n shares which are random elements of a finite field. Any set

of at least t shares allow recovery of the secret value via Lagrange interpolation. Any non-qualifying set of shares looks randomly distributed, which provides perfect confidentiality. In this paper, we use $(2, 2)$ -Shamir secret sharing or simply additive secret sharing, which the two shares add up to the secret value in the field. Many S2C protocols operate on the shares (e.g., see [33]).

3 OUR CONSTRUCTION

3.1 Accelerated Triplet Generation

The convolutional and fully-connected layers involve many inner-product computations. For preserving privacy, \mathcal{S}_1 and \mathcal{S}_2 operate on the secret shares of the inputs. They first prepare a triplet for minimizing the cost of online computation over secret shares. Specifically, \mathcal{S}_1 holds a_1 and b_1 , \mathcal{S}_2 holds a_2 and b_2 . They would like to compute the multiplication of $a = a_1 + a_2$ and $b = b_1 + b_2$ in a shared form i.e., \mathcal{S}_1 obtains z_1 , \mathcal{S}_2 obtains z_2 where $z_1 + z_2 = ab$.

The triplets generation algorithm TRIP in Fig. 2 consists of time-consuming homomorphic operations. Since $ab = (a_1 + a_2)(b_1 + b_2) = a_1b_1 + a_1b_2 + a_2b_1 + a_2b_2$, we can compute a_1b_1 and a_2b_2 locally. To compute a_1b_2 and a_2b_1 , \mathcal{S}_1 first encrypts a_1 and b_1 and sends the ciphertexts to \mathcal{S}_2 . So, \mathcal{S}_2 can add V_1, V_2 , and a random number r together to obtain V_3 via additive homomorphism without information leakage. The shared result of \mathcal{S}_2 is $z_2 = a_2b_2 + r$. By decrypting V_3 , \mathcal{S}_1 obtains v , which is added to a_1b_1 to obtain the shared result z_1 . In this way, the shared results z_1 and z_2 can recover the multiplication result z by simple addition, but neither \mathcal{S}_1 nor \mathcal{S}_2 can learn z . This preparation is done in an offline stage.

The triplet generation process involves many homomorphic operations. To further speed up the triplet generation process, we also adopt data packing and asynchronous computation.

3.1.1 Data Packing

Considering n shares $\langle a_1^i, b_1^i, a_2^i, b_2^i \rangle_{i=1}^n$, we pack $\langle a_1^i \rangle_{i=1}^n$ together to be a single plaintext A_1 to generate n triplets simultaneously. Analogously, we compute the packed data $B_1 = \langle b_1^i \rangle_{i=1}^n$, $A_2 = \langle a_2^i \rangle_{i=1}^n$, and $B_2 = \langle b_2^i \rangle_{i=1}^n$. The homomorphic operations are then performed on the packed data via SIMD [29] to get the packed triplets $((A_1, A_2), (B_1, B_2), (Z_1, Z_2))$. They can then be unpacked to extract the real triplets $\langle (a_1^i, a_2^i), (b_1^i, b_2^i), (z_1^i, z_2^i) \rangle_{i=1}^n$, where $z_1^i + z_2^i = (a_1^i + a_2^i) \cdot (b_1^i + b_2^i)$. In essence, our approach reduces the encryption, transmission, addition, and multiplication costs. Fig. 4 gives a toy example for the packed triplet generation process.

3.1.2 Asynchronous Computation

In the offline phase, \mathcal{S}_1 and \mathcal{S}_2 have to wait for the intermediate results from the other while generating the triplets. We call this synchronous computation, as demonstrated on the left of Fig. 5. To speed it up, we design an asynchronous computation scheme exhibited on the right of Fig. 5. Instead of waiting for the feedback, the servers continue the remaining operations which do not involve the feedback. For example, \mathcal{S}_1 can encrypt b_1 when transforming the ciphertext a_1 . \mathcal{S}_2 can encrypt the random

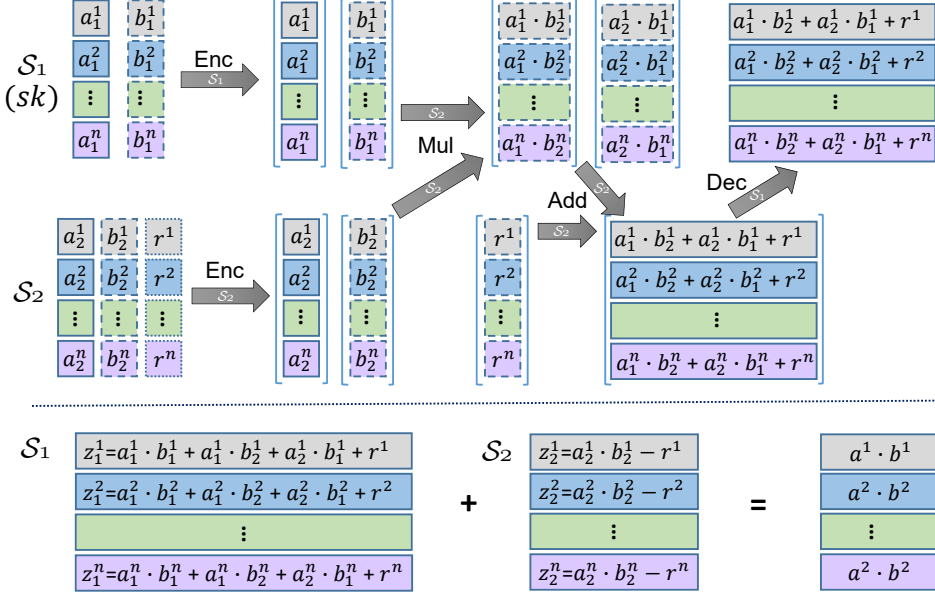


Fig. 4: Packed triplet generation process

number r and compute $a_2 b_2$ ahead of time. Compared with synchronous computing, asynchronous computation reduces the waiting time and hence the latency.

3.2 Our Design

With reference to the system overview in Fig. 1, our system consists of the following stages.

3.2.1 Initialization

\mathcal{S}_1 possesses one share of the prediction model, *i.e.*, the convolutional kernel C^1 and the weight matrix W^1 , and the HE key pair (pk, sk) . \mathcal{S}_2 owns the other share of the prediction model (*i.e.*, C^2 and W^2) and the public key pk . \mathcal{U} holds the query image \mathcal{G} .

3.2.2 Secret-Sharing the Query

\mathcal{U} randomly divides the pixel $\mathcal{G}_{i,j}$ ($i, j \in [1, n]$) of query \mathcal{G} into $\mathcal{G}_{i,j}^1$ and $\mathcal{G}_{i,j}^2$ as $\mathcal{G}_{i,j} = \mathcal{G}_{i,j}^1 + \mathcal{G}_{i,j}^2$. \mathcal{G}^1 and \mathcal{G}^2 are distributed to \mathcal{S}_1 and \mathcal{S}_2 , respectively.

3.2.3 Convolution Computation

As in Fig. 3, \mathcal{S}_1 and \mathcal{S}_2 first extract the sub-image $\tilde{\mathcal{G}}_{i,j}^1$ and $\tilde{\mathcal{G}}_{i,j}^2$ with the size of $m \times m$ from the shared images \mathcal{G}^1 and \mathcal{G}^2 , respectively. They then engage in the TRIP protocol to generate $\text{tri} = ((A_1, A_2), (B_1, B_2), (Z_1, Z_2))$. With tri , \mathcal{S}_1 (\mathcal{S}_2) uses A_1 (A_2) as a one-time pad to hide the sub-images $\tilde{\mathcal{G}}_{i,j}^1$ (*resp.* $\tilde{\mathcal{G}}_{i,j}^2$). Likewise, they use B_1 (B_2) to hide the convolutional kernel C^1 (*resp.* C^2). After they exchanged these padded shares, they can locally compute \mathcal{H}^1 and \mathcal{H}^2 . $\mathcal{H}^1 + \mathcal{H}^2$ gives

$$\begin{aligned} Z_1 + Z_2 + \tilde{\mathcal{G}}_{i,j} V + CU - (\tilde{\mathcal{G}}_{i,j} - A)(C - B) \\ = AB + \tilde{\mathcal{G}}_{i,j} C - \tilde{\mathcal{G}}_{i,j} B + \tilde{\mathcal{G}}_{i,j} C - CA \\ - (\tilde{\mathcal{G}}_{i,j} C - AC - \tilde{\mathcal{G}}_{i,j} B + AB) = \mathcal{G}_{i,j} \cdot C. \end{aligned}$$

3.2.4 Activation Computation

\mathcal{S}_1 and \mathcal{S}_2 use the garbled circuit in Fig. 6 to compute the activation function over \mathcal{H}^1 and \mathcal{H}^2 . The circuit utilizes four sub-circuits:

- $\text{ADD}(a, b)$ outputs the sum $a + b$;
- $\text{GT}(a, b)$ returns the bit denoting if $a > b$;
- $\text{MUX}(a, b, c)$ outputs a or b according to c , *i.e.*, if c holds, $\text{MUX}(a, b, c) = b$, otherwise $\text{MUX}(a, b, c) = a$; and
- $\text{SUB}(a, b)$ returns the difference $a - b$.

(ActF): $((0/1) \cdot \mathcal{H} - R; R) \leftarrow \text{ActF}(\mathcal{H}^1; (\mathcal{H}^2, R))$, \mathcal{S}_1 and \mathcal{S}_2 run ActF with \mathcal{H}^1 and (\mathcal{H}^2, R) being the respective inputs, where R is a random matrix generated by \mathcal{S}_2 . The outputs of \mathcal{S}_1 and \mathcal{S}_2 are $(0/1) \cdot \mathcal{H} - R$ and R , respectively. Specifically, $\text{ADD}(\mathcal{H}^1, \mathcal{H}^2)$ adds \mathcal{H}^1 and \mathcal{H}^2 to get \mathcal{H} . Then $\text{GT}(\mathcal{H}, 0)$ compares \mathcal{H} and 0 element-wise for ReLU. The output is a binary matrix B of the same size as \mathcal{H} , where the pixel $B_{i,j} = 1$ if $\mathcal{H}_{i,j} > 0$, 0 otherwise. With B , $\text{MUL}(\mathcal{H}, 0, B)$ performs activation function, *i.e.*, if $\mathcal{H}_{i,j} > 0$ ($B_{i,j} = 1$), outputs \mathcal{H} , otherwise outputs 0. Finally, SUB makes element-wise subtraction to have $B \cdot \mathcal{H} - R$, which is the output of \mathcal{S}_1 . Let \mathcal{J} be the activated image $B \cdot \mathcal{H}$. $\mathcal{J}^1 = B \cdot \mathcal{H} - R$. The output of \mathcal{S}_2 is regarded as $\mathcal{J}^2 = R$.

3.2.5 Pooling Computation

The two servers can perform the average-pooling on the respective shared data (*e.g.*, \mathcal{J}^1 and \mathcal{J}^2) without any interaction.

$$\begin{aligned} &(\mathcal{J}_1^1 + \mathcal{J}_2^1 + \dots + \mathcal{J}_{q^2}^1)/q^2 + (\mathcal{J}_1^2 + \mathcal{J}_2^2 + \dots + \mathcal{J}_{q^2}^2)/q^2 \\ &= (\mathcal{J}_1 + \mathcal{J}_2 + \dots + \mathcal{J}_{q^2})/q^2. \end{aligned}$$

Fig. 7 shows how \mathcal{S}_1 and \mathcal{S}_2 perform element-wise average-pooling over $(\mathcal{J}^1, \mathcal{J}^2)$ to obtain $(\mathcal{K}^1, \mathcal{K}^2)$. The pixel value $\mathcal{K}_{i,j}^1$ is the average of the corresponding $q \times q$ pixels in \mathcal{J}^1 . Analogously, $\mathcal{K}_{i,j}^2$ can be derived from \mathcal{J}^2 . Employing the average value to replace the original pixels, we can reduce \mathcal{J} to the down-sampled image \mathcal{K} of size $\lceil \frac{n}{q} \rceil \times \lceil \frac{n}{q} \rceil$.

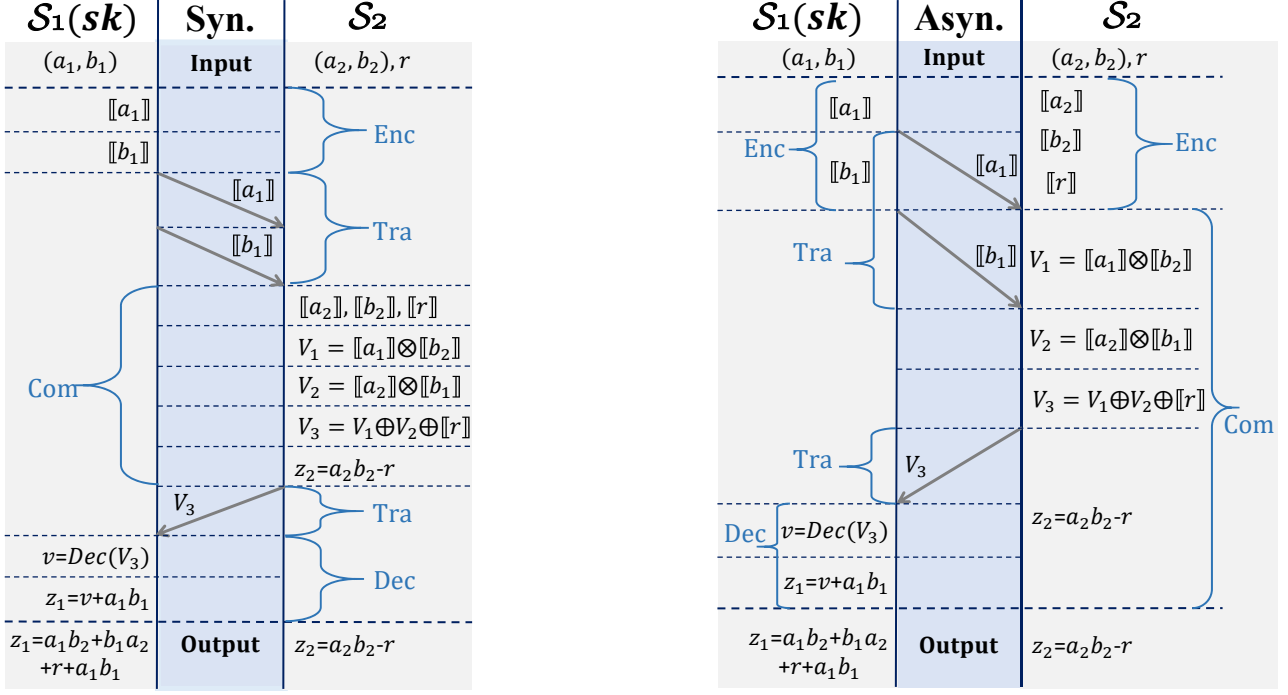


Fig. 5: Synchronous and asynchronous computations

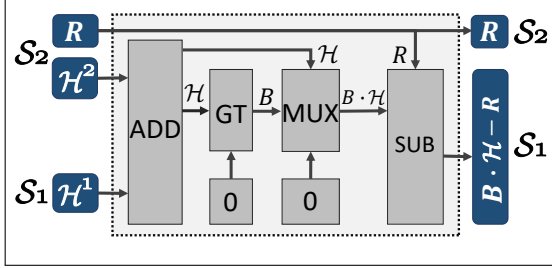


Fig. 6: Activation function circuit

$$(\mathcal{K}^1; \mathcal{K}^2) \leftarrow \text{POOL}(\mathcal{J}^1; \mathcal{J}^2)$$

Input: \mathcal{S}_1 holds the shared activated image \mathcal{J}_1 , \mathcal{S}_2 holds the other shares \mathcal{J}_2 .

Output: \mathcal{S}_1 obtains the shared pooled image \mathcal{K}_1 , \mathcal{S}_2 holds the other share \mathcal{K}_2 .

At \mathcal{S}_1 side:

- 1) **for** i, j **in range** $\lfloor \frac{n}{q} \rfloor$
 - Compute $\frac{1}{q \times q} \sum_{u=0}^{u=q-1} \sum_{v=0}^{v=q-1} \mathcal{J}_{qi-u, qj-v}^1$.
 - Set the averages as the value of $\mathcal{K}_{i,j}^1$.

At \mathcal{S}_2 side:

- 1) **for** i, j **in range** $\lfloor \frac{n}{q} \rfloor$
 - Compute $\frac{1}{q \times q} \sum_{u=0}^{u=q-1} \sum_{v=0}^{v=q-1} \mathcal{J}_{qi-u, qj-v}^2$.
 - Set the averages as the value of $\mathcal{K}_{i,j}^2$.

Fig. 7: Pooling operation

3.2.6 Fully Connected Layer

This layer in essence performs dot products between the pooled data \mathcal{K} and the weight parameters W , which can be

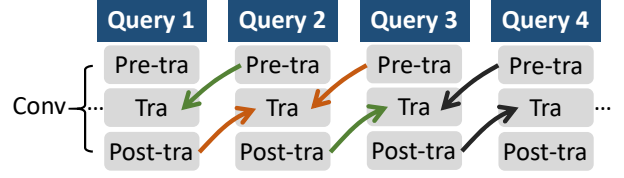


Fig. 8: Online asynchronous computation

computed using the triplets similar to that in the convolutional layer illustrated in Fig. 3. We skip the largely repetitive details. Specifically, \mathcal{S}_1 and \mathcal{S}_2 take as input the shares \mathcal{K}^1, W^1 and \mathcal{K}^2, W^2 respectively, resulting in the shared prediction results \mathcal{F}^1 and \mathcal{F}^2 . User \mathcal{U} can merge \mathcal{F}^1 and \mathcal{F}^2 to recover the result $\mathcal{F} = \mathcal{K}W$.

3.3 Accelerated Asynchronous Online Computations

For convolution and fully-connected layers, we can conduct computations (of U^1, V^1, U^2, V^2 (pre-transmission), $U, V, \mathcal{H}_{i,j}^1, \mathcal{H}_{i,j}^2$ (post-transmission)) and transmission (of U^1, V^1, U^2, V^2) at the same time. Fig. 8 illustrates the asynchronous computation process. The computation process at the tail of the arrow is in parallel with the transmission process at the arrow head. For example, the pre-transmission and post-transmission operations of query 2 are in parallel with the transmission of query 1 and query 3, respectively.

4 PERFORMANCE EVALUATION

4.1 Experimental Setup and Dataset

Our experiments used MNIST dataset [34], a widely-used dataset in the machine learning community, which consists

- 1) *Convolution*: input image 28×28 , window size 5×5 , stride $(1, 1)$, number of output channels of 16: $\mathbb{R}^{16 \times 576} \leftarrow \mathbb{R}^{16 \times 25} \times \mathbb{R}^{25 \times 576}$.
- 2) *ReLU Activation*: calculates ReLU for each input.
- 3) *Average Pooling*: window size $1 \times 2 \times 2$ and outputs $\mathbb{R}^{16 \times 12 \times 12}$.
- 4) *Convolution*: input image 12×12 , window size 5×5 , stride $(1, 1)$, number of output channels of 16: $\mathbb{R}^{16 \times 64} \leftarrow \mathbb{R}^{16 \times 400} \times \mathbb{R}^{400 \times 64}$.
- 5) *ReLU Activation*: calculates ReLU for each input.
- 6) *Average Pooling*: window size $1 \times 2 \times 2$ and outputs $\mathbb{R}^{16 \times 4 \times 4}$.
- 7) *Fully Connected*: fully connects the incoming 256 notes to the outgoing 100 nodes: $\mathbb{R}^{100 \times 1} \leftarrow \mathbb{R}^{100 \times 256} \times \mathbb{R}^{256 \times 1}$.
- 8) *ReLU Activation*: calculates ReLU for each input.
- 9) *Fully Connected*: fully connects the incoming 100 notes to the outgoing 10 nodes: $\mathbb{R}^{10 \times 1} \leftarrow \mathbb{R}^{10 \times 100} \times \mathbb{R}^{100 \times 1}$.

Fig. 9: The neural network architecture used in our experiment

of 60,000 training and 10,000 black-white hand-written digit test-images of 28×28 pixels belong to 10 classes. Following MiniONN [12], we trained and implemented a realistic neural network. Fig. 9 details its architecture.

For \mathcal{U} , \mathcal{S}_1 , and \mathcal{S}_2 , we use separate machines with an Intel 4-Core CPU operating at 1.60 GHz and equipped with 8 GB RAM, running a ubuntu 18.04 operating system.

We implemented our scheme in C++ with Python binding. For garbled circuits, we use the ABY library with SIMD circuits [33]. Following MiniONN, we use YASHE for FHE and implement it by the SEAL library [35], which supports SIMD. In YASHE, the degree of the polynomial n is set to be 4096. In this way, we can pack 4096 elements together. The plaintext modulus is 101,285,036,033. The length of the plaintext is 64-bit. The ciphertext modulus is 128-bit. These parameters matter in Section 4.3.

All results are averaged over at least 5 runs, in which the error is controlled within 3%.

4.2 Accuracy Evaluation

4.2.1 Effect of Pooling Method

To evaluate average-pooling we used and max-pooling used in existing works, we trained the model with both methods. Fig. 10 and Fig. 11 plot the accuracy against the number of iterations for average-pooling and max-pooling, respectively. The light blue line P_1 represents the accuracy of the specific training epoch, where $P_1(i) (0 < i \leq 10000)$ is the accuracy after the i -th iteration. The sky blue line P_2 shows the smoothed accuracy $P_2(i) = \alpha P_2(i-1) + (1-\alpha)P_1(i)$, with the smoothing factor α set to 0.6. The dark blue line P_3 shows the accuracy on the test dataset.

The accuracy grows with the iterations until stabilized. After 1,000 iterations, the accuracy of max-pooling achieves 98.1% while that of average-pooling is just 97.5%. Yet, after 10,000 iterations, both the accuracy of the two methods can achieve 99.2%. In brief, although the

TABLE 3: Comparison of triplet generation

Methodology	Complexity	Required operations
SecureML [26]	$\mathcal{O}(n)$	$n \cdot (5\text{Enc} + 2\text{CMul} + 2\text{Add} + 1\text{Dec})$
MiniONN [12]	$\mathcal{O}(n/l)$	$\frac{n}{l} \cdot (5\text{Enc} + 2\text{CMul} + 2\text{Add} + 1\text{Dec})$
Our Scheme	$\mathcal{O}(n/l)$	$\frac{n}{l} \cdot (5\text{Enc} + 2\text{CMul} + 2\text{Add} + 1\text{Dec})$

Enc: encryption; CMul: constant multiplication between ciphertext and plaintext; Add: addition between two ciphertexts; Dec: decryption.

TABLE 4: Triplet generation costs

SecureML [26]	Our scheme with Acceleration	Our scheme with Asyn. Comp.	Performance Gain
79716.524ms	19.635ms	16.970ms	4697x

convergence of the average-pooling is relatively slow, the final accuracy is comparable or even higher than that of max-pooling.

4.2.2 Effect of Activation Function

Some FHE-based schemes [10], [19] approximate the activation function by polynomials. Fig. 12 plots the curves of the original ReLU function and its approximations with different degrees, which are polynomial regression function *polyfit* from the Python package numpy.

The approximation is satisfactory when the absolute value of the input is smaller than 4. However, for larger input, the error introduced by the approximate become very large, which makes the accuracy reduction noticeable. Our scheme reaches the same accuracy as plaintext computation by directly designing the garbled circuits for ReLU, which compute an identical output as ReLU.

4.3 Efficiency Evaluation

4.3.1 Triplet Generation

Table 3 compares our triplets generation method with prior work in terms of the complexity and the number of operations. As Fig. 2, triplet generation for two n -dimensional shared vectors of SecureML [26] encrypts each element of the shared vector respectively. This process consists of $5n$ Enc encryptions, $2n$ CMul multiplications and additions, n decryptions, in which n ciphertexts are transferred between the two servers. The complexity is $\mathcal{O}(n)$.

In contrast, MiniONN [12] and our scheme use the packing technique. All the l elements can be computed at the same time. The n -dimensional vector is compressed into an (n/l) -dimensional vector. This means that the complexity of MiniONN and our scheme is just $\mathcal{O}(n/l)$.

Table 4 shows that our accelerated triplet generation scheme enjoys several order-of-magnitude improvements over SecureML [26], for 4096 triplets. Further adopting asynchronous computations improves the efficiency to 13.6%, resulting in an overall speed up of 4697 times.

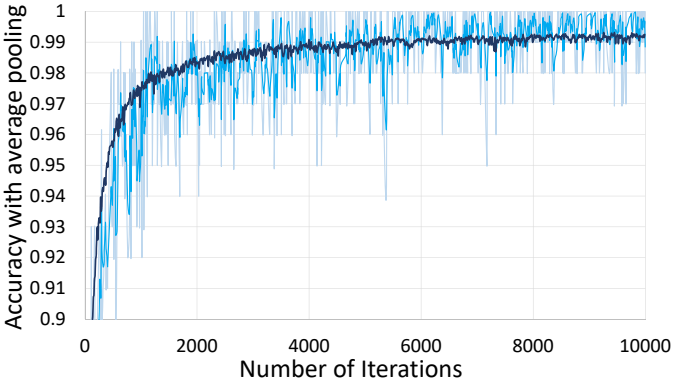


Fig. 10: Accuracy with average-pooling

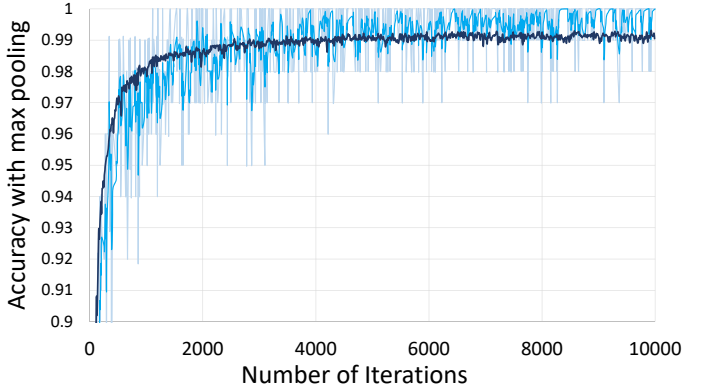


Fig. 11: Accuracy with max-pooling

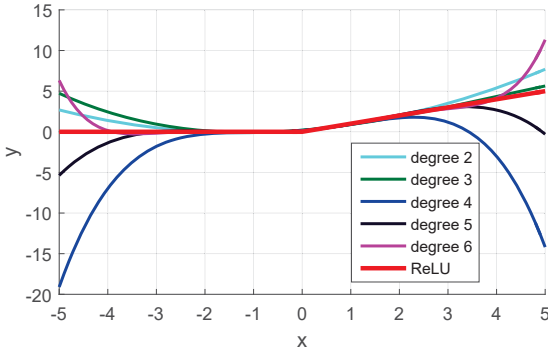


Fig. 12: Approximate of the ReLU function

TABLE 5: ReLU costs (ms)

	Offline	Online	Avg. Offline	Avg. Online
S_1	87.815	752.545	0.021	0.184
S_2	100.143	516.413	0.024	0.126

4.3.2 Activation Function

To make our contribution stand out, we run the activation function circuits alone to demonstrate its performance. Table 5 summarizes our results. We perform our RuLU with the SIMD circuits and activate the 4096 data simultaneously. For the packed data, the offline time costs for generating the circuits are 87.815ms and 100.143ms, respectively. The time consumptions in the online stage are 752.545ms and 516.413ms. The time costs are for 4096 pieces of data. The average per-data time costs of the offline and online computations are 0.045ms and 0.310ms.

Compared with the existing works using approximate polynomials, our GC-based circuits also provide higher efficiency. Table 6 illustrates the approximation polynomial with different degrees. If the degree is set to be 6, the approximation polynomial is $0.1249 + 0.5000x + 0.3729x^2 - 0.0410x^4 + 0.0016x^6$. When executing this polynomial, 13 multiplications and 4 addition are involved, which take 82.20ms. Therefore, our ReLU circuits outperform the approximation polynomial by 265 times.

TABLE 6: Polynomial approximation

Approximate Function	Time (ms)	Performance Gain
$0.1992 + 0.5002x + 0.1997x^2$	19.02	61 \times
$0.1995 + 0.5002x + 0.1994x^2 - 0.0164x^3$	38.00	123 \times
$0.1500 + 0.5012x + 0.2981x^2 - 0.0004x^3 - 0.0388x^4$	69.62	225 \times
$0.1488 + 0.4993x + 0.3007x^2 + 0.0003x^3 - 0.0168x^4$	69.64	224 \times
$0.1249 + 0.5000x + 0.3729x^2 - 0.0410x^4 + 0.0016x^6$	82.20	265 \times

4.3.3 Evaluation on MNIST

Table 7 reports the total latency for 4096 images and the amortized time for each image. In the offline phase, the two servers interact with each other to prepare the triplets, which costs about 2000s. The amortized time for each image is thus 0.487s. In the online phase, the activation function dominates since it uses garbled circuits. For the convolution layer, pooling layer, and fully connected layer, all the computations are executed over shares without HE or garbled circuits, which just takes a little time. Notably, the client just needs 2.197 μ s to encode the query and decode the prediction result. The amortized online time cost for the user is 3.284s.

4.3.4 Evaluation on Different Network Architectures

We conduct experiment over network architectures in four published works [26], [10], [14], [12], which use a combination of FC and Conv layers as follows. For FC($784 \rightarrow 128$), 784 and 128 respectively represent the size of the input and the output. On the other hand, for Conv($1 \times 28 \times 28 \rightarrow 5 \times 13 \times 13$), the input image is of size 28×28 with 1 channel, the output image is of size 13×13 with 5 channels. For the square activation function, it is essentially multiplication operation between two secret shares. In our scheme, we can achieve it by using the triplet, which is similar to the convolutional operation.

- Network1 [26]: FC($784 \rightarrow 128$) \Rightarrow Square \Rightarrow FC($128 \rightarrow 128$) \Rightarrow Square \Rightarrow FC($128 \rightarrow 10$).

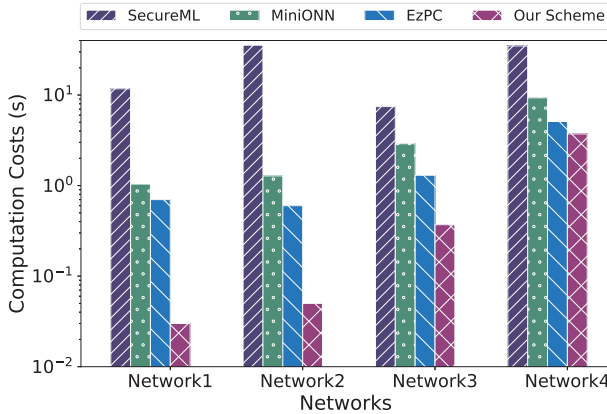


Fig. 13: Computation costs

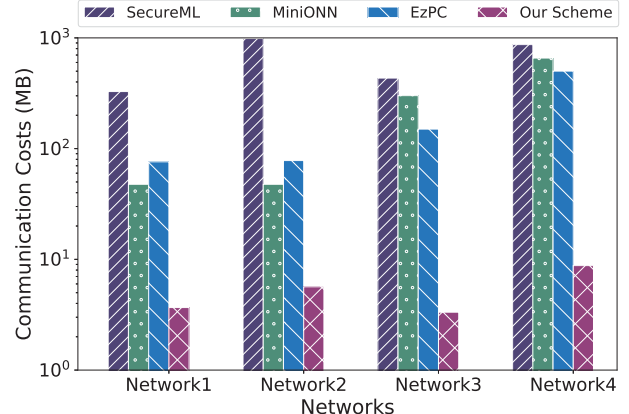


Fig. 14: Communication costs

TABLE 7: Performance in each phase

Phases		Latency (s)	Amortized time per image (s)
Offline	\mathcal{S}_1	913.735	0.223
	\mathcal{S}_2	1084.340	0.264
Online	Query Encoding	0.005	0.000
	Conv	268.932	0.065
	ReLU	11694.716	2.855
	Pooling	0.182	0.000
	Conv	29.881	0.007
	ReLU	1299.412	0.317
	Pooling	0.020	0.000
	Fully	29.876	0.007
	ReLU	126.895	0.031
	Result Decoding	0.004	0.000
	Total	13451.094	3.284

- Network2 [10]: Conv($1 \times 28 \times 28 \rightarrow 5 \times 13 \times 13$) \Rightarrow Square \Rightarrow Pooling($5 \times 13 \times 13 \rightarrow 5 \times 13 \times 13$) \Rightarrow Conv ($5 \times 13 \times 13 \rightarrow 50 \times 5 \times 5$) \Rightarrow Pooling($50 \times 5 \times 5 \rightarrow 50 \times 5 \times 5$) \Rightarrow FC($1250 \rightarrow 100$) \Rightarrow Square \Rightarrow FC($100 \rightarrow 10$).
- Network3 [14]: Conv($1 \times 28 \times 28 \rightarrow 5 \times 13 \times 13$) \Rightarrow ReLU \Rightarrow FC($845 \rightarrow 100$) \Rightarrow ReLU \Rightarrow FC($100 \rightarrow 10$).
- Network4 [12]: the same as the one in Section 4.1.

Table 8 shows the performance of synchronous and asynchronous computations in both the offline and online phases. For network1, the total time cost of the existing schemes with synchronous computation is 0.040s while the time cost of our scheme with asynchronous computation is just 0.029. In other words, we obtain 27.5 % performance saving. Analogously, the savings for network2, network3, and network4 are 20.0%, 1.7%, 1.4% respectively. In short, our asynchronous computation reduces the latency.

To demonstrate the superiority of our scheme, we

compare with SecureML [26], MiniONN [12], and EzPC [15]. Fig. 13 and Fig. 14 show the computation and communication costs on different neural network architectures, respectively. Compared with SecureML [26] (with model privacy), we provide $282\times$ faster computation time and $122\times$ lower communication cost. Compared with MiniONN [12] (without model privacy), our scheme performs $18\times$ and $49\times$ better. Compared with EzPC [15] (without model privacy), ours is $10\times$ and $38\times$ better.

5 SECURITY ANALYSIS

Both the query and the model are randomly shared and distributed to two independent servers. As long as they do not collude, the privacy of the query and the model are preserved. For the intermediate data and the results, both servers possess the corresponding share with pre-computed triplets, which are independent of the sensitive data. The query, the model, the intermediate data, and the prediction results are secret-shared. Hence no meaningful information is revealed to the semi-honest servers.

We provide simulation-based proof for security under the semi-honest model.

Security Definition: Let $f = (f_{\mathcal{U}}, f_{\mathcal{S}_1}, f_{\mathcal{S}_2})$ be a probabilistic polynomial function and \prod a protocol computing f . The user and two servers want to compute $f(\mathcal{G}, \mathcal{C}^1, \mathcal{C}^2, \mathcal{W}^1, \mathcal{W}^2)$ using \prod where \mathcal{G} is the query image of the user \mathcal{U} , and $(\mathcal{C}^1, \mathcal{W}^1)$ and $(\mathcal{C}^2, \mathcal{W}^2)$ are the shared model deposited on the two servers. The view of \mathcal{U} during the execution of \prod is $V_{\mathcal{U}}(\mathcal{G}, \mathcal{C}^1, \mathcal{C}^2, \mathcal{W}^1, \mathcal{W}^2) = (\mathcal{G}, r_{\mathcal{U}}, m_{\mathcal{U}})$ where $r_{\mathcal{U}}$ is the random tape of \mathcal{U} , and $m_{\mathcal{U}}$ is the message received by \mathcal{U} . Simultaneously, the view of \mathcal{S}_1 and \mathcal{S}_2 are defined as $V_{\mathcal{S}_1}(\mathcal{G}, \mathcal{C}^1, \mathcal{C}^2, \mathcal{W}^1, \mathcal{W}^2) = (\mathcal{C}^1, \mathcal{W}^1, r_{\mathcal{S}_1}, m_{\mathcal{S}_1})$, $V_{\mathcal{S}_2}(a, b, c) = (\mathcal{C}^2, \mathcal{W}^2, r_{\mathcal{S}_2}, m_{\mathcal{S}_2})$. The protocol \prod achieving the function f is regarded as secure if for every possible input $\mathcal{G}, \mathcal{C}^1, \mathcal{C}^2, \mathcal{W}^1, \mathcal{W}^2$ of f , there exist the probabilistic polynomial time simulators $\Phi_{\mathcal{U}}, \Phi_{\mathcal{S}_1}$, and $\Phi_{\mathcal{S}_2}$ such that,

$$\begin{aligned} \Phi_{\mathcal{U}}(a, f_{\mathcal{U}}(\mathcal{G}, \mathcal{C}^1, \mathcal{C}^2, \mathcal{W}^1, \mathcal{W}^2)) &\equiv_p V_{\mathcal{U}}(\mathcal{G}, \mathcal{C}^1, \mathcal{C}^2, \mathcal{W}^1, \mathcal{W}^2), \\ \Phi_{\mathcal{S}_1}(a, f_{\mathcal{S}_1}(\mathcal{G}, \mathcal{C}^1, \mathcal{C}^2, \mathcal{W}^1, \mathcal{W}^2)) &\equiv_p V_{\mathcal{S}_1}(\mathcal{G}, \mathcal{C}^1, \mathcal{C}^2, \mathcal{W}^1, \mathcal{W}^2), \\ \Phi_{\mathcal{S}_2}(a, f_{\mathcal{S}_2}(\mathcal{G}, \mathcal{C}^1, \mathcal{C}^2, \mathcal{W}^1, \mathcal{W}^2)) &\equiv_p V_{\mathcal{S}_2}(\mathcal{G}, \mathcal{C}^1, \mathcal{C}^2, \mathcal{W}^1, \mathcal{W}^2), \end{aligned}$$

where \equiv_p denotes computational indistinguishability.

TABLE 8: Performance of the synchronous computation and asynchronous computation on different networks

	Network 1		Network 2		Network 3		Network 4	
	Syn. Comp	Asyn. Comp						
Offline Phase (s)	0.007	0.005	0.020	0.016	0.052	0.050	0.492	0.489
Online Phase (s)	0.033	0.023	0.050	0.039	0.323	0.319	3.285	3.234
Total (s)	0.040	0.028	0.070	0.057	0.375	0.368	3.777	3.723

Theorem 1: The triplet generation protocol in Section 3.1 is secure against semi-honest adversaries.

Proof: \mathcal{S}_1 holds the secret key. All the messages passed from \mathcal{S}_1 to \mathcal{S}_2 are encrypted. All those passed from \mathcal{S}_2 to \mathcal{S}_1 are distributed uniformly by adding random data independent of the data of \mathcal{S}_2 . The view of \mathcal{S}_1 is $V_{\mathcal{S}_1} = (C^1, W^1, a_1, b_1, z_1)$, where a_1, b_1, z_1 come from the triplet of \mathcal{S}_1 . We construct the simulator $\Phi_{\mathcal{S}_1}(C^1, W^1)$ as:

- 1) Pick the random integers $\hat{a}_1, \hat{b}_1, \hat{z}_1$ from \mathbb{Z}_{2^t} .
- 2) Output $\Phi_{\mathcal{S}_1}(C^1, W^1) = (C^1, W^1, \hat{a}_1, \hat{b}_1, \hat{z}_1)$.

As the randomness \hat{a}_1 (or \hat{b}_1, \hat{z}_1) is generated in the same manner as a_1 (or a_1, b_1), and independent from the other data, the distribution of $(C^1, W^1, \hat{a}_1, \hat{b}_1, \hat{z}_1)$ and $(C^1, W^1, a_1, b_1, z_1)$ are indistinguishable. Thus we have proven that $V_{\mathcal{S}_1} \equiv_p \Phi_{\mathcal{S}_1}(C^1, W^1)$. Analogously, $\Phi_{\mathcal{S}_2}(C^2, W^2) = (C^2, W^2, \hat{a}_2, \hat{b}_2, \hat{z}_2)$, $V_{\mathcal{S}_2} \equiv_p \Phi_{\mathcal{S}_2}(C^2, W^2)$.

Theorem 2: The image distribution protocol in Section 3.2.2 is secure against semi-honest adversaries.

Proof: User \mathcal{U} additively shares the query image into two parts. The views of the three parties are $V_{\mathcal{U}} = (\mathcal{G}, R_{\mathcal{G}})$, $V_{\mathcal{S}_1} = (C^1, W^1, \mathcal{G}^1)$, $V_{\mathcal{S}_2} = (C^2, W^2, \mathcal{G}^2)$, where $\mathcal{G}^1 = R_{\mathcal{G}}$, $\mathcal{G}^2 = \mathcal{G} - R_{\mathcal{G}}$. We construct a simulator $\Phi_{\mathcal{S}_1}(C^1, W^1)$ as:

- 1) Pick random integers $\hat{R}_{\mathcal{G}}$ from \mathbb{Z}_{2^t} and set $\hat{\mathcal{G}}^1 = \hat{R}_{\mathcal{G}}$.
- 2) Output $\Phi_{\mathcal{S}_1}(C^1, W^1) = (C^1, W^1, \hat{\mathcal{G}}^1)$.

Both $R_{\mathcal{G}}$ and $\hat{R}_{\mathcal{G}}$ are generated randomly. Hence the distribution of $R_{\mathcal{G}}$ and $\hat{R}_{\mathcal{G}}$ are indistinguishable. As a consequence, we have $V_{\mathcal{S}_1} \equiv_p \Phi_{\mathcal{S}_1}(C^1, W^1)$. Analogously, $\Phi_{\mathcal{S}_2}(C^2, W^2) = (C^2, W^2, \hat{\mathcal{G}}^2)$, $V_{\mathcal{S}_2} \equiv_p \Phi_{\mathcal{S}_2}(C^2, W^2)$.

Theorem 3: The convolutional computation protocol in Section 3.2.3 is secure against semi-honest adversaries.

Proof: The two servers perform the convolution with the help of triplets. Their views $V_{\mathcal{S}_1}$ and $V_{\mathcal{S}_2}$ are $(C^1, W^1, \mathcal{G}^1, \mathcal{H}^1, A_1, B_1, Z_1)$, $(C^2, W^2, \mathcal{G}^2, \mathcal{H}^2, A_1, B_1, Z_1)$ respectively. We construct a simulator $\Phi_{\mathcal{S}_1}(C^1, W^1)$ as:

- 1) Call the triplet generation protocol to have $\hat{A}_1, \hat{B}_1, \hat{Z}_1$.
- 2) Pick the random integers $\hat{\mathcal{G}}^1, \hat{U}^2, \hat{V}^2$ from \mathbb{Z}_{2^t} .
- 3) Compute $\hat{U} = \hat{\mathcal{G}}^1 - \hat{A}_1 + \hat{U}^2, \hat{V} = C^1 - \hat{B}_1 + \hat{V}^2$.
- 4) Compute $\hat{\mathcal{H}}^1 = -\hat{U}\hat{V} + \hat{\mathcal{G}}^1\hat{V} + C^1\hat{U} + \hat{Z}_1$.
- 5) Output $\Phi_{\mathcal{S}_1}(C^1, W^1) = (C^1, W^1, \hat{\mathcal{G}}^1, \hat{\mathcal{H}}^1)$.

The distribution of \mathcal{H}^1 and $\hat{\mathcal{H}}^1$ are indistinguishable. Hence $V_{\mathcal{S}_1} \equiv_p \Phi_{\mathcal{S}_1}(C^1, W^1)$ holds. Analogously, we have $\Phi_{\mathcal{S}_2}(C^2, W^2) = (C^2, W^2, \hat{\mathcal{G}}^2, \hat{\mathcal{H}}^2)$, and $V_{\mathcal{S}_2} \equiv_p \Phi_{\mathcal{S}_2}(C^2, W^2)$.

Theorem 4: The activation computation protocol in Section 3.2.4 is secure against semi-honest adversaries.

Proof: The two servers compute the activation function by using the designed garbled circuits. The view of \mathcal{S}_1 is $V_{\mathcal{S}_1} = (C^1, W^1, \mathcal{H}^1, \mathcal{J}^1)$. The view of \mathcal{S}_2 is $V_{\mathcal{S}_2} = (C^2, W^2, \mathcal{H}^2, \mathcal{J}^2)$. Since the garbled circuits are

secure against semi-honest adversaries, we only consider the inputs and outputs of the circuits rather than the internal details. We construct a simulator $\Phi_{\mathcal{S}_1}(C^1, W^1)$ as:

- 1) Pick the random integers $\hat{\mathcal{H}}^1, \hat{\mathcal{J}}^1$ from \mathbb{Z}_{2^t} .
- 2) Output $\Phi_{\mathcal{S}_1}(C^1, W^1) = (C^1, W^1, \hat{\mathcal{H}}^1, \hat{\mathcal{J}}^1)$.

The distributions of \mathcal{H}^1 (\mathcal{J}^1) and $\hat{\mathcal{H}}^1$ ($\hat{\mathcal{J}}^1$) are indistinguishable. Hence $V_{\mathcal{S}_1} \equiv_p \Phi_{\mathcal{S}_1}(C^1, W^1)$ holds. Analogously, we have $\Phi_{\mathcal{S}_2}(C^2, W^2) = (C^2, W^2, \hat{\mathcal{H}}^2, \hat{\mathcal{J}}^2)$, and $V_{\mathcal{S}_2} \equiv_p \Phi_{\mathcal{S}_2}(C^2, W^2)$.

Theorem 5: The pooling computation protocol in Section 3.2.5 is secure against semi-honest adversaries.

Proof: The view of \mathcal{S}_1 is $V_{\mathcal{S}_1} = (C^1, W^1, \mathcal{J}^1, \mathcal{K}^1)$. The view of \mathcal{S}_2 is $V_{\mathcal{S}_2} = (C^2, W^2, \mathcal{J}^2, \mathcal{K}^2)$. We construct a simulator $\Phi_{\mathcal{S}_1}(C^1, W^1)$ as:

- 1) Pick the random integers $\hat{\mathcal{J}}^1, \hat{\mathcal{K}}^1$ from \mathbb{Z}_{2^t} .
- 2) Output $\Phi_{\mathcal{S}_1}(C^1, W^1) = (C^1, W^1, \hat{\mathcal{J}}^1, \hat{\mathcal{K}}^1)$.

Since the distribution of \mathcal{J}^1 (\mathcal{K}^1) and $\hat{\mathcal{J}}^1$ ($\hat{\mathcal{K}}^1$) are indistinguishable, $V_{\mathcal{S}_1} \equiv_p \Phi_{\mathcal{S}_1}(C^1, W^1)$ holds. Analogously, $\Phi_{\mathcal{S}_2}(C^2, W^2) = (C^2, W^2, \hat{\mathcal{J}}^2, \hat{\mathcal{K}}^2)$, and $V_{\mathcal{S}_2} \equiv_p \Phi_{\mathcal{S}_2}(C^2, W^2)$.

Theorem 6: The fully connected protocol in Section 3.2.6 is secure against semi-honest adversaries.

Proof: The views $V_{\mathcal{S}_1}$ and $V_{\mathcal{S}_2}$ are $(C^1, W^1, \mathcal{K}^1, \mathcal{F}^1, A_1, B_1, Z_1)$, $(C^2, W^2, \mathcal{K}^2, \mathcal{F}^2, A_2, B_2, Z_2)$ respectively. We construct a simulator $\Phi_{\mathcal{S}_1}(C^1, W^1)$ as:

- 1) Call the triplet generation protocol to have $\hat{A}_1, \hat{B}_1, \hat{Z}_1$.
- 2) Pick the random integers $\hat{\mathcal{K}}^1, \hat{U}^2, \hat{V}^2$ from \mathbb{Z}_{2^t} .
- 3) Compute $\hat{U} = \hat{\mathcal{K}}^1 - \hat{A}_1 + \hat{U}^2, \hat{V} = W^1 - \hat{B}_1 + \hat{V}^2$.
- 4) Compute $\hat{\mathcal{F}}^1 = -\hat{U}\hat{V} + \hat{\mathcal{K}}^1\hat{V} + W^1\hat{U} + \hat{Z}_1$.
- 5) Output $\Phi_{\mathcal{S}_1}(C^1, W^1) = (C^1, W^1, \hat{\mathcal{K}}^1, \hat{\mathcal{F}}^1)$.

The distribution of \mathcal{F}^1 and $\hat{\mathcal{F}}^1$ are indistinguishable. Hence $V_{\mathcal{S}_1} \equiv_p \Phi_{\mathcal{S}_1}(C^1, W^1)$ holds. Analogously, we have $\Phi_{\mathcal{S}_2}(C^2, W^2) = (C^2, W^2, \hat{\mathcal{K}}^2, \hat{\mathcal{F}}^2)$, and $V_{\mathcal{S}_2} \equiv_p \Phi_{\mathcal{S}_2}(C^2, W^2)$.

6 ADDITIONAL RELATED WORKS

Wang *et al.* [36] focused on natural language processing and proposed a secure model learning method under the non-colluding assumptions. Bost *et al.* [37] considered various machine-learning classifications (e.g., hyperplane decision-based classifiers, naïve Bayes classifiers, decision trees) over FHE-encrypted data. Tai *et al.* [18] proposed privacy-preserving decision-trees evaluation by modelling the decision tree with linear functions, so additive homomorphic encryption suffices. Using multi-key FHE, Aloufi *et al.* [21] considered secure outsourcing of decision-trees evaluation. One may refer to a brief overview of Chow [38] for the state-of-the-art in

privacy-preserving decision-tree evaluation. All these works did not consider neural networks.

For some latest and representative works for neural network evaluation in the S2C setting without model privacy, EzPC [15] proposes a compiler that translates between arithmetic and boolean circuits. XONN [16] “replaces” the matrix multiplication with XNOR, which is virtually free in GC. Yet, this scheme only applies to the binary neural networks, *i.e.*, the parameters are binary. DeepSecure [14] preprocesses the data and network before S2C but leaks some information about the parameters.

Differential privacy [39], [40], [41] adds noise without sacrificing too much data utility, but it cannot wholly ensure data privacy. Trusted processor (*e.g.*, Intel SGX) approaches [42], [43], [44], [45] work on the data within the trusted perimeter, but they are subjected to the memory constraint (currently 128MB) which can be easily exceeded by a specific layer of a deep neural network. Moreover, paging introduces overhead. Cryptographic approaches, in general, do not have these problems.

7 CONCLUSION

We improve the accuracy and efficiency of neural network prediction that preserves privacy in the outsourcing setting (*i.e.*, the servers providing the prediction service can get nothing about the query, the model, any intermediate results, and the final result). We adopt non-linear activate function which preserves the accuracy of the underlying neural network. We also reduce both the computation and communication overheads by adopting packing and asynchronous computation. Extensive experiments show that our scheme outperforms the state-of-the-art.

REFERENCES

- [1] I. Goodfellow, Y. Bengio, and A. Courville, *Deep Learning*. MIT Press, 2016, <http://www.deeplearningbook.org>.
- [2] Y. Adi, C. Baum, M. Cissé, B. Pinkas, and J. Keshet, “Turning your weakness into a strength: Watermarking deep neural networks by backdooring,” in *USENIX Security Symposium*, 2018, pp. 1615–1631.
- [3] R. Shokri, M. Stronati, C. Song, and V. Shmatikov, “Membership inference attacks against machine learning models,” in *IEEE Symposium on Security and Privacy (S&P)*, 2017, pp. 3–18.
- [4] J. Hayes, L. Melis, G. Danezis, and E. D. Cristofaro, “LOGAN: membership inference attacks against generative models,” *PoPETs*, vol. 2019, no. 1, pp. 133–152, 2019.
- [5] A. Salem, Y. Zhang, M. Humbert, P. Berrang, M. Fritz, and M. Backes, “ML-Leaks: Model and data independent membership inference attacks and defenses on machine learning models,” in *ISOC Network and Distributed System Security Symposium (NDSS)*, 2019.
- [6] N. Papernot, P. D. McDaniel, I. J. Goodfellow, S. Jha, Z. B. Celik, and A. Swami, “Practical black-box attacks against machine learning,” in *ACM Asia Conference on Computer and Communications Security (AsiaCCS)*, 2017, pp. 506–519.
- [7] J. Jia and N. Z. Gong, “AttriGuard: A practical defense against attribute inference attacks via adversarial machine learning,” in *USENIX Security Symposium*, 2018, pp. 513–529.
- [8] G. F. Elsayed, S. Shankar, B. Cheung, N. Papernot, A. Kurakin, I. J. Goodfellow, and J. Sohl-Dickstein, “Adversarial examples that fool both computer vision and time-limited humans,” in *Neural Information Processing Systems (NeurIPS)*, 2018, pp. 3914–3924.
- [9] Z. Wang, M. Song, S. Zheng, Z. Zhang, Y. Song, and Q. Wang, “Invisible adversarial attack against deep neural networks: An adaptive penalization approach,” *IEEE Trans. Dependable Sec. Comput.*, 2019, early access.
- [10] R. Gilad-Bachrach, N. Dowlin, K. Laine, K. E. Lauter, M. Naehrig, and J. Wernsing, “CryptoNets: Applying neural networks to encrypted data with high throughput and accuracy,” in *International Conference on Machine Learning (ICML)*. ACM, 2016, pp. 201–210.
- [11] H. Chabanne, A. de Wargny, J. Milgram, C. Morel, and E. Prouff, “Privacy-preserving classification on deep neural network,” *IACR Cryptology ePrint Archive* 2017/035, 2017.
- [12] J. Liu, M. Juuti, Y. Lu, and N. Asokan, “Oblivious neural network predictions via MiniONN transformations,” in *ACM Conference on Computer and Communications Security (CCS)*, 2017, pp. 619–631.
- [13] C. Juvekar, V. Vaikuntanathan, and A. Chandrakasan, “GAZELLE: A low latency framework for secure neural network inference,” in *USENIX Security Symposium*, 2018, pp. 1651–1669.
- [14] B. D. Rouhani, M. S. Riazi, and F. Koushanfar, “DeepSecure: scalable provably-secure deep learning,” in *Design Automation Conference (DAC)*, 2018, pp. 2:1–2:6.
- [15] N. Chandran, D. Gupta, A. Rastogi, R. Sharma, and S. Tripathi, “EzPC: Programmable, efficient, and scalable secure two-party computation,” in *EuroS&P*. IEEE, 2019, pp. 496–511.
- [16] M. S. Riazi, M. Samragh, H. Chen, K. Laine, K. E. Lauter, and F. Koushanfar, “XONN: XNOR-based oblivious deep neural network inference,” in *USENIX Security Symposium*, 2019, pp. 1501–1518.
- [17] C. Gentry, “Fully homomorphic encryption using ideal lattices,” in *Symposium on Theory of Computing (STOC)*. ACM, 2009, pp. 169–178.
- [18] R. K. H. Tai, J. P. K. Ma, Y. Zhao, and S. S. M. Chow, “Privacy-preserving decision trees evaluation via linear functions,” in *European Symposium on Research in Computer Security (ESORICS)*, 2017, pp. 494–512.
- [19] E. Hesamifard, H. Takabi, M. Ghasemi, and R. N. Wright, “Privacy-preserving machine learning as a service,” *PoPETs*, vol. 2018, no. 3, pp. 123–142, 2018.
- [20] X. Jiang, M. Kim, K. E. Lauter, and Y. Song, “Secure outsourced matrix computation and application to neural networks,” in *ACM Conference on Computer and Communications Security (CCS)*, 2018, pp. 1209–1222.
- [21] A. Aloufi, P. Hu, H. W. H. Wong, and S. S. M. Chow, “Blindfolded evaluation of random forests with multi-key homomorphic encryption,” *IEEE Trans. Dependable Sec. Comput.*, 2019, early access.
- [22] S. S. M. Chow, J. Lee, and L. Subramanian, “Two-party computation model for privacy-preserving queries over distributed databases,” in *ISOC Network and Distributed System Security Symposium (NDSS)*, 2009.
- [23] S. Kamara, P. Mohassel, and M. Raykova, “Outsourcing multiparty computation,” *IACR Cryptology ePrint Archive* 2011/272.
- [24] B. Wang, M. Li, S. S. M. Chow, and H. Li, “A tale of two clouds: Computing on data encrypted under multiple keys,” in *IEEE Conference on Communications and Network Security, CNS*, 2014, pp. 337–345.
- [25] M. Baryalai, J. Jang-Jaccard, and D. Liu, “Towards privacy-preserving classification in neural networks,” in *Privacy, Security and Trust (PST)*, 2016, pp. 392–399.
- [26] P. Mohassel and Y. Zhang, “SecureML: A system for scalable privacy-preserving machine learning,” in *IEEE Symposium on Security and Privacy (S&P)*. IEEE, 2017, pp. 19–38.
- [27] D. Beaver, “Efficient multiparty protocols using circuit randomization,” in *Advances in Cryptology – CRYPTO*, 1991, pp. 420–432.
- [28] A. C. Yao, “How to generate and exchange secrets,” in *IEEE Symposium on Foundations of Computer Science*. IEEE, 1986, pp. 162–167.
- [29] N. P. Smart and F. Vercauteren, “Fully homomorphic SIMD operations,” *Des. Codes Cryptography*, vol. 71, no. 1, pp. 57–81, 2014.
- [30] Q. Zou, Z. Zhang, Q. Li, X. Qi, Q. Wang, and S. Wang, “Deepcrack: Learning hierarchical convolutional features for crack detection,” *IEEE Trans. Image Processing*, vol. 28, no. 3, pp. 1498–1512, 2019.
- [31] J. W. Bos, K. E. Lauter, J. Loftus, and M. Naehrig, “Improved security for a ring-based fully homomorphic encryption scheme,” in *IMA Int'l Conference on Cryptography and Coding (IMACC)*, 2013, pp. 45–64.
- [32] A. Shamir, “How to share a secret,” *Commun. ACM*, vol. 22, no. 11, pp. 612–613, 1979.

- [33] D. Demmler, T. Schneider, and M. Zohner, "ABY - A framework for efficient mixed-protocol secure two-party computation," in *ISOC Network and Distributed System Security Symposium (NDSS)*, 2015.
- [34] Y. LeCun, "The MNIST database of handwritten digits," <http://yann.lecun.com/exdb/mnist>, 1998.
- [35] N. Dowlin, R. Gilad-Bachrach, K. Laine, K. E. Lauter, M. Naehrig, and J. Wernsing, "Manual for using homomorphic encryption for bioinformatics," *Proc. of the IEEE*, vol. 105, no. 3, pp. 552–567, 2017.
- [36] Q. Wang, M. Du, X. Chen, Y. Chen, P. Zhou, X. Chen, and X. Huang, "Privacy-preserving collaborative model learning: The case of word vector training," *IEEE Trans. Knowl. Data Eng.*, vol. 30, no. 12, pp. 2381–2393, 2018.
- [37] R. Bost, R. A. Popa, S. Tu, and S. Goldwasser, "Machine learning classification over encrypted data," in *ISOC Network and Distributed System Security Symposium (NDSS)*, 2015.
- [38] S. S. M. Chow, "Privacy-preserving machine learning (Invited paper)," in *Frontiers in Cyber Security. FCS 2018*, ser. Communications in Computer and Information Science, vol. 879. Springer, 2018.
- [39] M. Abadi, A. Chu, I. J. Goodfellow, H. B. McMahan, I. Mironov, K. Talwar, and L. Zhang, "Deep learning with differential privacy," in *ACM Conference on Computer and Communications Security (CCS)*, 2016, pp. 308–318.
- [40] A. D. Smith, A. Thakurta, and J. Upadhyay, "Is interaction necessary for distributed private learning?" in *IEEE Symposium on Security and Privacy (S&P)*, 2017, pp. 58–77.
- [41] L. Xiang, J. Yang, and B. Li, "Differentially-private deep learning from an optimization perspective," in *IEEE International Conference on Computer Communications (INFOCOM)*, 2019, pp. 559–567.
- [42] O. Ohrimenko, F. Schuster, C. Fournet, A. Mehta, S. Nowozin, K. Vaswani, and M. Costa, "Oblivious multi-party machine learning on trusted processors," in *USENIX Security Symposium*, 2016, pp. 619–636.
- [43] T. Hunt, C. Song, R. Shokri, V. Shmatikov, and E. Witchel, "Chiron: Privacy-preserving machine learning as a service," *CoRR*, 2018, abs/1803.05961.
- [44] S. Hu, L. Y. Zhang, Q. Wang, Z. Qin, and C. Wang, "Towards private and scalable cross-media retrieval," *IEEE Trans. Dependable Sec. Comput.*, 2019, early access.
- [45] F. Tramèr and D. Boneh, "Slalom: Fast, verifiable and private execution of neural networks in trusted hardware," in *International Conference on Learning Representations (ICLR)*, 2019.



Minghui Li received her B.S. degree in Information Security in 2016, and her M.S. degree in Computer Technology in 2018, from Wuhan University, China. She is currently pursuing the Ph.D. degree in the School of Cyber Science and Engineering, Wuhan University, China. Her research focuses on security and privacy issues in cloud computing and artificial intelligence.



Sherman S. M. Chow received his Ph.D. degree from New York University. He is an associate professor with the Chinese University of Hong Kong. He was a research fellow with the University of Waterloo. His interest is applied cryptography. He has published in AsiaCrypt, CCS, EuroCrypt, ITCS, NDSS, and Usenix Security. He served on the program committees of many conferences including AsiaCrypt, CCS, CRYPTO, CTRSA, Financial Crypt, ICDCS, Infocom, PETS, PKC, and TheWeb. He has also served on the editorial board of many journals and book series, including IEEE TRANS. INFORMATION FORENSICS AND SECURITY (TIFS), IET Information Security (IET-IFS), Intl. J. Information Security (IJIS), J. of Information Security and Applications (JISA), EAI Endorsed Transactions on Scalable Information Systems, and SpringerBriefs on Cyber Security Systems and Networks (CSSN). He is a European Alliance for Innovation (EAI) Fellow (2019, inaugural), and named as one of the 100 Most Influential Scholars (Security and Privacy, 2018) by ArnetMiner (AMiner). He received the Early Career Award from the Hong Kong Research Grants Council.



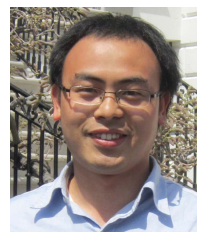
Shengshan Hu received the B.E. degree from Wuhan University, China, in 2014, in Computer Science and Technology. He is currently a PhD candidate in the School of Cyber Science and Engineering in Wuhan University. His research interest focuses on secure outsourcing of computations.



Yuejing Yan received her B.S. and M.S. degrees from Wuhan University, China. She is currently pursuing the Ph.D. degree in the State Key Laboratory of Information Engineering in Surveying, Mapping, and Remote Sensing, Wuhan University, China. Her research interest focuses on secure outsourcing of computation.



Minxin Du received his B.S. and M.S. degrees in Information Security from Wuhan University. He is now a Ph.D. student with the Chinese University of Hong Kong. His research focuses on applied cryptography.



Zhibo Wang received the B.E. degree in Automation from Zhejiang University, China, in 2007, and his Ph.D. degree in Electrical Engineering and Computer Science from University of Tennessee, in 2014. He is currently a Professor with the School of Cyber Science and Engineering, Wuhan University, China. His current research interests include Internet of Things, network security and privacy protection. He is an IEEE Senior Member and an ACM Member.